Journal of Magnetism and Magnetic Materials 86 (1990) 254–260
North-Holland

THE EFFECT OF ELECTRON BEAM CURRENT IN SEM ON THE OBSERVED DOMAIN STRUCTURE OF METALLIC GLASSES

K. ZÁVĚTA, K. JUREK, V. KAMBERSKÝ, P. KRÁL

Institute of Physics, Czechoslovak Academy of Sciences, Na Slovance 2, 180 40 Prague 8, Czechoslovakia

and

H. LACHOWICZ

Institute of Physics, Polish Academy of Sciences, Al. Lotników 32/46, 02-668 Warsaw, Poland

Received 1 August 1989; in revised form 23 October 1989

An excessive increase of the intensity of electron beam current in the scanning electron microscope may lead to a distinct change of the magnetic domain structure observed by means of type II magnetic contrast. This effect was studied on two types of amorphous alloys, one with very low and the other with a rather large positive magnetostriction. From the calculations of the heating effect of the electron beam together with the analysis of the experiments, it was concluded that the results may be explained by the local anisotropy induced by the strain distribution around the area heated by the beam, favouring a normal component of magnetization close to the surface and consequently an associated closure domain pattern.

1. Introduction

During our previous studies of magnetic domain structures in amorphous alloys by means of a scanning electron microscope, we mentioned the influence of the primary electron beam current upon the observed structure at the sample surface [1]. In the present work we report on a more detailed investigation of this effect in two different types of metallic glasses under various conditions, including the observation at elevated temperatures. The experimental results indicate that the observed effects are caused by local heating and thermal strain in the beam area. To support this hypothesis we describe simple model calculations of temperature and strain distributions, and discuss the observed domain structures in connection with strain-induced magnetic anisotropy.

2. Experimental details

The materials used in our investigation were produced by single-roller quenching in the form of ribbons whose thicknesses were 30 μm and widths equalled 6 or 10 mm. Their compositions were $Co_{67}Fe_4Cr_7Si_8B_{14}$ and $Co_{55}Fe_5Ni_{14}Si_{16}B_{10}$, representative of metallic glasses with low magnetostriction and decreased Curie temperature, and $Ni_{40}Fe_{40}B_{20}$ for a typical magnetically soft material with a considerably high magnetostriction constant. The latter material was prepared by flow-casting in vacuum and its surface was of a rather good quality. The low-magnetostriction materials were annealed under tensile stress which resulted in creep-induced anisotropy [2], with the easy plane normal to the stress axis and essentially stripe-domain structure with zig-zag shaped domain walls [3].

The domain structures on the surface of our samples were observed by means of JEOL JXA 733 Superprobe Scanning Electron Microscope using the type II magnetic contrast (see ref. [1] for references; the thickness of the imaged surface layer is about 2–3 μm). When elevated temperatures were required, the sample was mounted on a heated stage that enabled us to work at temperatures up to 250 °C. Another special sample holder

0304-8853/90/$03.50

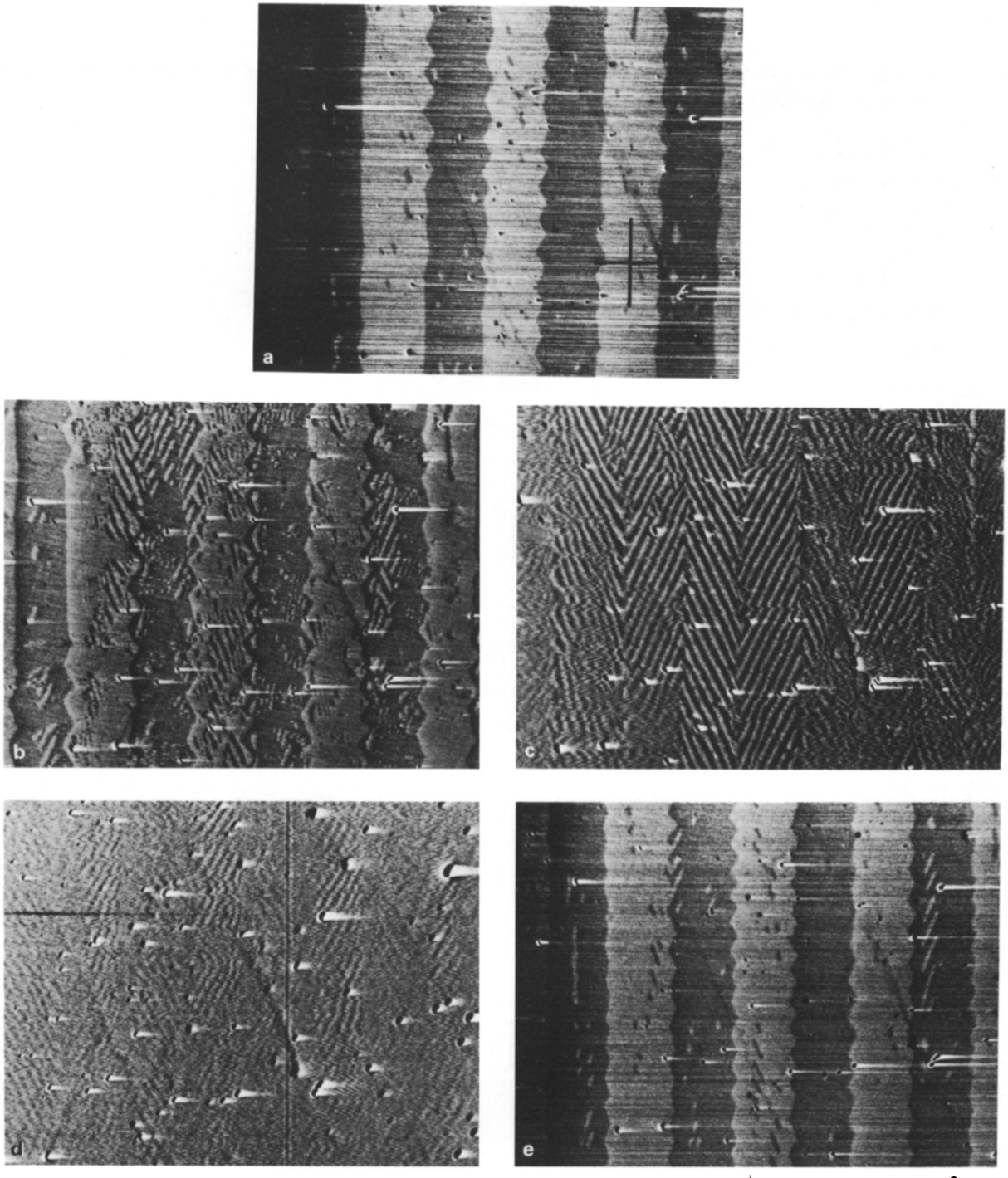

Fig. 1. The domain structure of $Co_{67}Fe_4Cr_7Si_3B_{14}$ observed by SEM with various primary electron beam currents: (a) 4×10^{-8} A; (b) 11×10^{-8} A; (c) 25×10^{-8} A; (d) 45×10^{-8} A; (e) 4×10^{-8} A. The cross indicates 0.1 mm.

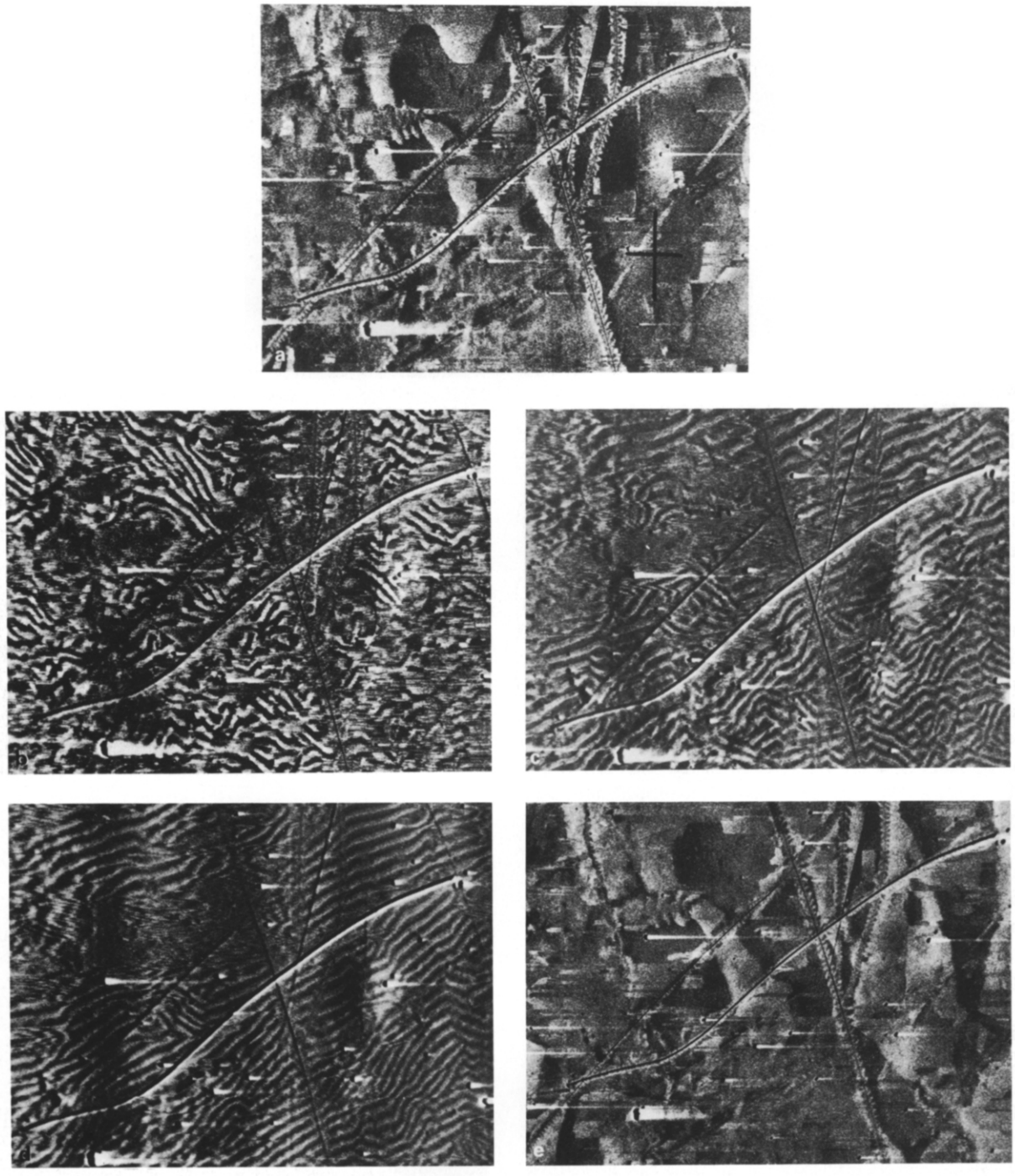

Fig. 2. The domain structure of $Ni_{40}Fe_{40}B_{20}$ with various primary electron beam currents: (a) 6×10^{-8} A; (b) 20×10^{-8} A; (c) 40×10^{-8} A; (d) 60×10^{-8} A; (e) 6×10^{-8} A. The cross indicates 0.1 mm.

made it possible to apply the magnetic field in the ribbon plane, the maximum field being several times higher than the field necessary for saturation. Domains were observed on the shiny (free) surface of samples electrocut from the ribbon; the surface was neither polished nor etched.

3. Experimental results

The domain structures of the low-magnetostriction material observed at primary electron beam currents from 4 to 45×10^{-8} A and accelerating voltage of 50 kV are shown in figs. 1a–e (imaging always the same area of the sample). The original wide stripes with zig-zag walls gradually disintegrate with increasing current into chevrons and subsequently into even finer patterns; at sufficiently high current the magnetic contrast entirely disappears. The original, only slightly changed, structure reappears upon returning to the lower current. It is worth noting that even under the fine structure, the original positions of the stripes are discernible.

The changes (with increasing current) of the surface domain structure of the material with higher magnetostriction differ in character as seen from figs. 2a–e. The initial irregular structure decays into randomly interwoven fine stripes which become more regular at higher beam intensity. After decreasing the primary current, the structure of the original type reappears but is not reproduced in detail.

In order to explain the observed changes, we considered two possible effects of the beam impinging on the sample surface, (i) magnetic field produced by the beam in its immediate vicinity; (ii) heating of the sample by the absorbed beam energy.

The magnetic field of an electron beam of diameter $d = 10^{-7}$ m carrying the current $I_b = 10^{-6}$ A is of the order of 1 A/m at the beam circumference, which might be high enough to affect local magnetization. To test this possibility we performed the following experiment: the beam current I_b was increased at constant accelerating voltage $U_{a_1} = 50$ kV until marked changes appeared in the observed domain structure. Then U_a was decreased to 30 kV at constant I_{b_1} (i.e. constant magnetic field of the beam). This resulted in partial recovery of the original (wide-stripe) structure. Finally, at $U_{a_2} = 30$ kV, I_b was further increased until fine-structure features comparable to those seen previously at U_{a_1} reappeared; it was established that this occurs when $U_{a_2} I_{b_2} \sim U_{a_1} I_{b_1}$, i.e., at approximately the same power of the beam. Another indication that the magnetic field of the beam is not decisive for the described changes comes from the observation that external magnetic fields applied to the sample moved the walls but did not alter the effects of the primary beam current.

Uniform external heating of the sample (on the heated stage) resulted in a lower magnetic contrast, due to the decrease of magnetization, but produced no indication of transition to the finer domain structure. We are thus led to the conclusion that the local character of the heating by the beam is important; this is also indicated by the observation that, with higher speed of the scan, the critical beam current, at which the magnetic contrast disappeared, was increased.

Intuitively, we expect that the local heating produces expansion mainly in the direction normal to the surface, which may lead to significant magnetoelastic effects. To assess such effects quantitatively, we need an analysis of spatial distributions of the temperature and strain produced by the beam.

4. Model calculations

The energy of the electron beam is absorbed in a rather sharply localized pear-shaped region lying directly below the surface [4]; with the materials and beam powers used in our experiments its dimensions are a few μm. For the sake of computational simplicity, we represent this region by a hemisphere centered at the surface, in which the absorbed power density is uniform. Due to essentially metallic heat conductivity, $\lambda \approx 1$ to 10 W/Km [5], in a first approximation we may neglect radiation losses and solve the equation of heat conduction with the upper sample surface insulated.

For long expositions in a standing beam (scanning velocity $v = 0$) we get, for thick samples, the asymptotic spherically symmetric stationary solutions for the distribution of the temperature increment $T(r)$

$$\frac{T(r)}{T_0} = \begin{cases} 1 - \frac{1}{3}\left(\frac{r}{r_0}\right)^2, & r < r_0, \\ \frac{2}{3}\frac{r_0}{r}, & r > r_0, \end{cases} \tag{1}$$

where $t = 0$ corresponds to the ambient temperature, r_0 is the radius of the heated hemisphere; the sample thickness, much larger than r_0, is increased to infinity, and T_0 is the maximum temperature,

$$T_0 = \frac{3W}{4\pi r_0 \lambda}, \tag{2}$$

where $W = U_a I_b$ denotes the absorbed power. With $W \approx 5$ mW we thus find $T_0 \approx 10^2$ to 10^3 K.

The initial increase of T, for very short exposures of duration t, is linear in t inside the heated volume,

$$T = \frac{3W}{2\pi r_0^3 c} t, \quad r < r_0$$

(and $T = 0$ outside); this may be written as

$$T/T_0 = t/t_0 \tag{3}$$

with the characteristic time

$$t_0 = r_0^2 c/2\lambda, \tag{4}$$

where $c(\approx 2 \times 10^6$ J/Km^3 [5]) denotes the heat capacity per unit volume; the same t_0 characterizes the initial cooling rate when the beam is switched off. With the above parameters we find $t_0 \approx 0.1$ to 1 μs. This is very short compared to the local exposition time in the scanning regime, $t_e = 2r_0/v$ where $v = d/t_f$, $d \approx 0.1$ to 1 mm is the scanned length and $t_f = 40$ ms is the line scanning time. Eq. (4) is only valid for $t \ll t_0$, while for $t > t_0$ the solutions approach saturation given by eq. (1). Hence, in the described experiments we may expect temperature distributions around the instantaneous beam positions closely resembling the stationary solution (1).

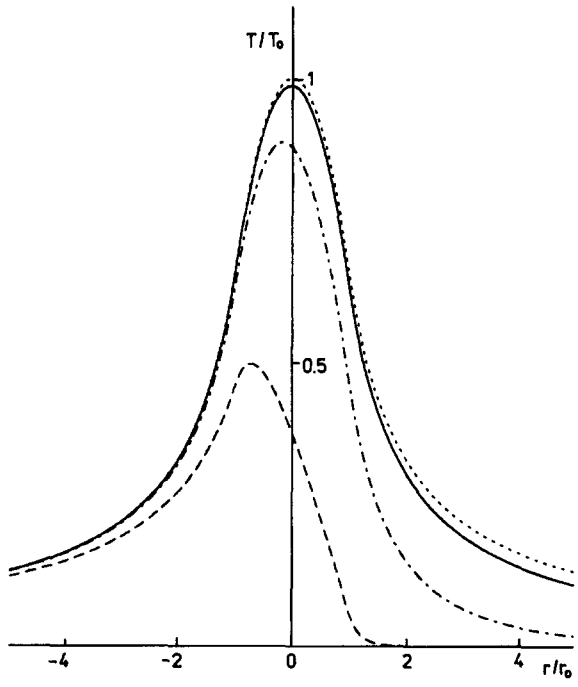

Fig. 3. Dependence of the temperature increment T on the distance r from the centre of the beam spot computed along the scanning path at various velocities: $v/v_0 = 0$ (dotted), 0.01 (solid), 0.1 (dot-dashed) and 1 (dashed); T_0, r_0 and v_0 are defined in the text.

This conclusion is corroborated by numerical solutions of the heat-conduction problem performed for the hemispherical heat source, moving with various velocities v for a fixed time t_f (fig. 3). Significant departures from the stationary temperature distribution are found when v approaches the critical value $v_0 = 2r_0/t_0$ or,

$$v_0 = 4\lambda/cr_0, \tag{5}$$

which is about 100 times higher than the highest v attained in our experiments. Further approximations taking into account the opposite sample surface were also investigated numerically. Since r_0 is much smaller than the sample thickness, the local gradient of T around the beam spot is little affected; the long-range "tail" described as r_0/r in eq. (1) is slightly enhanced or diminished (for insulated or cooled bottom surface, respectively).

The thermal strain resulting from the local heating was computed from the equations of elas-

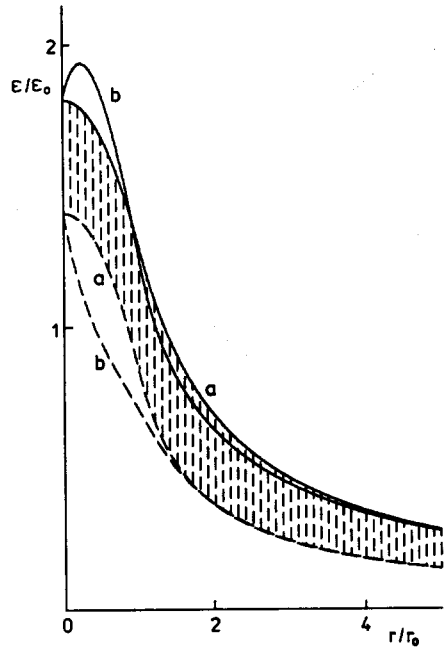

Fig. 4. Dependence of the components of the strain tensor, ϵ_{zz} (solid) and $\epsilon_{\parallel} = (\epsilon_{xx} + \epsilon_{yy})/2$ (dashed), with z along the surface normal, on the distance r from the centre of the beam spot: (a) r in the surface plane (lines joined by hatching); (b) r along the normal; ϵ_0 and r_0 are defined in the text.

tic equilibrium [6] in several steps: first, assuming the spherically symmetric $T(r)$ of eq. (1) in the whole space, which leads to non-vanishing stress, τ^s_{zz}, in the plane $z = 0$ of the sample surface; this stress is then relaxed (i.e., the strain resulting from an external surface pressure $-\tau^s_{zz}$ is added to the spherical solution). All components of the strain tensor ϵ_{ij} were computed numerically as functions of the depth (z) and lateral distance (x) from the center of the beam spot. The essential features of the results are presented in fig. 4 which shows two sections of this dependence: on z at $x = 0$ and on x at $z = 0$. The plots are in units of

$$\epsilon_0 = \frac{1}{3}\frac{1+\nu}{1-\nu}\alpha T_0 \qquad (6)$$

(where $\nu \approx 0.3$ is the elastic Poisson constant and α is the linear thermal expansion coefficient) i.e., essentially, in units of the maximum linear expansion at T_0 of eq. (2). Along with the normal component ϵ_{zz} we have plotted the average in-plane strain $\epsilon_{\parallel} = (\epsilon_{xx} + \epsilon_{yy})/2$ since the difference $\epsilon_{zz} - \epsilon_{\parallel}$ is significant for the magnetoelastic anisotropy discussed further below. Fig. 4 shows that this difference is positive, its magnitude is comparable with ϵ_0 in the centre and falls off radially with a long-range tail, like the temperature in eq. (1). This is confirmed by additional calculations, indicating again that the other sample surface is of minor importance.

5. Discussion

Thermal expansion, prevalently in the direction normal to the sample surface, and the high positive magnetostriction of the $Fe_{40}Ni_{40}B_{20}$ alloy cause temporary uniaxial magnetic anisotropy with the easy axis normal to the surface. The effective anisotropy constant is then equal to $K_\perp = \frac{3}{2}\lambda_s E(\epsilon_{zz} - \epsilon_{\parallel})$ where λ_s is the saturation magnetostriction constant and E the Young modulus. The maximum $K_\perp$ near the beam spot is thus of order $K^0_\perp \sim \lambda_s \alpha T_0 E$ (cf. fig. 4 and eq. (6)); with $\lambda_s \gtrsim 10^{-5}$, $\alpha \approx 10^{-5}$, $T_0 \approx 10^2$ K and $E \gtrsim 100$ GPa we expect $K^0_\perp \gtrsim 10^3$ J m^{-3}. Such anisotropy is large enough to induce components of local magnetization perpendicular to the surface, provided that the magnetostatic energy of such configuration is reduced by alternating signs of the normal M_z components and by the formation of flux-closure domains. We thus presume that the fine chevron structures observed on the surface at high beam currents are just the closure domains (magnetized parallel to the surface, as follows from the theory of the type II magnetic contrast). The long ranges of both the strain (and anisotropy) distributions and of the magnetostatic interaction may support structures of dimensions much larger than $2r_0$ (the diameter of the heated spot). The macroscopic coherence of the observed heat-induced structures, in particular, their reproduction in each line of the relatively slow scan, is presumably connected not only with local variation of residual anisotropy but also with the effective fields of the underlying equilibrium domain structure.

It should be noted that similar fine-striped structures were observed on similar materials by means of the Kerr effect [7,8], and generally inter-

preted as being due to local stress with normal components resulting from fluctuations in the process of the rapid quenching.

In our samples of the low-magnetostriction Co-based alloys, the presence of creep-induced anisotropy with an easy plane perpendicular to the ribbon surface is likely to diminish significantly the threshold value of the perpendicular anisotropy constant $K_\perp$ needed for the appearance of domains with normal magnetization components (and of the accompanying closure domains). This is indicated by an analysis of the experimental results concerning zig-zag wall structures (given in refs. [3,9] and to be published). Hence, we assume that even very low positive magnetostriction with $\lambda_s \lesssim 10^{-6}$ may produce the same type of effect as discussed above.

Our explanation of the observed effects as being essentially due to the anisotropy of thermal strain is supported by the results of preliminary experiments on samples with small but negative λ_s: at high beam currents, transitions to fine domain structure are not observed; on the other hand, fine-structure regions spontaneously existing (presumably due to local anisotropy normal to the surface), disappear.

References

[1] K. Závěta, K. Jurek and P. Duhaj, Czech. J. Phys. B37 (1987) 42.
[2] L. Kraus, N. Zárubová, K. Závěta and P. Duhaj, in: Magnetic Properties of Amorphous Metals, eds. A. Hernando, V. Madurga, M.C. Sanchez-Trujillo and M. Vázquez (North-Holland, Amsterdam, 1987) p. 206.
[3] K. Závěta, L. Kraus, K. Jurek and V. Kamberský, J. Magn. Magn. Mat. 73 (1988) 334.
[4] K. Murata, T. Matsukawa and R. Shimizu, Japan. J. Appl. Phys. 10 (1971) 684.
[5] P. Svoboda and P. Vašek, Phys. Stat. Sol. (a) 106 (1988) 115.
[6] L.D. Landau and E.M. Lifshitz, Teoria uprugosti (Moscow, 1965).
[7] B. Gröger and H. Kronmüller, J. Magn. Magn. Mat. 9 (1978) 203.
[8] J.D. Livingston, Phys. Stat. Sol. (a) 56 (1979) 637.
[9] R. Gemperle and I. Tomáš, J. Magn. Magn. Mat. 73 (1988) 339.